CrystEngComm

PAPER

View Article Online
View Journal | View Issue

Cite this: *CrystEngComm*, 2017, **19**, 4920

Computational screening of covalent organic frameworks for the capture of radioactive iodine and methyl iodide†

Youshi Lan,[a] Minman Tong,*[b] Qingyuan Yang *[a] and Chongli Zhong[a]

Received 17th January 2017,
Accepted 13th March 2017

DOI: 10.1039/c7ce00118e

rsc.li/crystengcomm

Effective capture of radioactive iodic contaminants from nuclear wastes is of great importance for public safety as well as the secure utility of nuclear energy. In this work, a computational study was performed to systematically evaluate the performance of 187 experimentally reported covalent organic frameworks (COFs) for gaseous I_2 and CH_3I adsorption under real industrial conditions. The results show that 3D-COFs present better performance than 2D-COFs for both I_2 and CH_3I adsorption. 3D-Py-COF was identified with the highest I_2 uptake of 16.7 g g^{-1}, outperforming the adsorbents reported to date. In addition, based on the obtained structure–property relationships, a new 3D-COF with an even higher I_2 uptake of 19.9 g g^{-1} was designed. For CH_3I adsorption, the pore morphology plays an important role, and 3D-COFs with **ctn** topology having a pore size of around 9 Å show superiority compared with other COFs. COF-103 was identified as the best material with a CH_3I uptake of 2.8 g g^{-1}, which is much higher than those of traditional adsorbents like activated carbons, alumina and zeolites.

Introduction

Considering the gradual exhaustion of fossil fuels and the intense requirement of greenhouse gas emission reduction, developing alternative clean and sustainable energy sources is viewed as crucial to secure worldwide economic prosperity and stability.[1] In this aspect, the promising nuclear energy offers cost-effective and non-carbon-emitting options compared to other types of energy sources. Currently, nuclear energy has provided about 13% of global electricity and the ratio is growing steadily to meet the rapidly increasing energy demands.[2] However, an urgent issue of safety concern behind nuclear power production is the control and management of generated radioactive wastes, the severe hazards of which can be reflected from the Chernobyl and Fukushima accidents. During the reprocessing operation of nuclear plants, there are various gaseous radionuclides of iodine in the released off-gas streams.[3,4] Particularly, ^{129}I is a highly volatile contaminant with an extraordinarily long half-life (~10^7 years), and its elemental (or molecular) form (I_2) is dangerous for the health of the general public and the environment.[5,6] Additionally, although the half-life of ^{131}I is only 8 days, it is the most abundant and usually combined with other hydrocarbons to yield organic compounds such as methyl iodide (CH_3I),[7] which also has serious impacts on the metabolic system of human beings.[8,9] Consequently, effective capture and storage of the two species remain strong concerns for public safety as well as the safe utility of nuclear energy.

Different methods are available for the removal of gaseous radioactive iodic contaminants, including precipitation, dry dedusting, wet scrubbing, adsorption, *etc.*[10] Among them, adsorption techniques based on porous adsorbents have been in the forefront due to their many advantages, such as high removal efficiency, low maintenance cost, simple equipment design and operation.[3] So far, various traditional porous media have been tried, such as activated carbons[11] and the TEDA- or DABCO-impregnated forms,[7,12] aerogels,[13,14] and clay materials.[15] Currently, the prevalent industrial approach for iodine capture is to use silver-exchanged zeolites (AgZ) as the adsorbents.[8] However, these materials have the drawbacks of low adsorption capacities and adverse environmental impact of silver.[16,17] Therefore, suitable adsorbents with a lower overall cost which can tackle issues of global importance are in high demand. Recently, both experimental and theoretical studies have been performed to investigate the performance of metal–organic frameworks (MOFs) for iodine capture.[18,19] For examples, Nenoff and co-workers[20–22] systematically studied the I_2 adsorption properties of Cu-BTC and ZIF-8 by combining computational and experimental

[a] *Beijing Advanced Innovation Center for Soft Matter Science and Engineering, Beijing University of Chemical Technology, Beijing 100029, China. E-mail: qyyang@mail.buct.edu.cn*

[b] *School of Chemistry and Chemical Engineering, Jiangsu Normal University, Xuzhou 221116, China. E-mail: tongmm@jsnu.edu.cn*

† Electronic supplementary information (ESI) available: A list of the COFs examined in this work and their structural features, force field parameters, the properties of the COFs identified with the best performance, and some comparison results. See DOI: 10.1039/c7ce00118e

methods; they found that the two MOFs behave much better compared to AgZ, exhibiting promising capability for I_2 capture application. Some experimental studies also suggested that MOFs decorated with functional moieties like amine[23,24] and thiol[25] groups can find better applications for the encapsulation of I_2. Assfour *et al.*[26] computationally screened a diverse set of 12 MOFs for I_2 capture at 298 K and found that the top material NU-110 shows a very high adsorption capacity (13 g g^{-1}) at 1 bar, which was claimed to be higher than any material capacity reported at that time. From a computational investigation of I_2 adsorption behaviour in 21 ZIFs, Yuan *et al.*[27] identified that ZIF-10 has the highest adsorption capacity (2.39 g g^{-1}) at 298 K and moderate pressures. As far as we know, there is no related work reported for evaluating the performance of MOFs towards CH_3I capture. More importantly, the existing studies on MOFs mainly focus on exploring their performance for iodine capture at ambient temperature or 348 K, while the more relevant operational temperature in the nuclear industry is around 423 K.[5]

Covalent organic frameworks (COFs) represent a novel class of crystalline nanoporous materials in which organic building units are assembled together to form periodic networks *via* strong covalent bonds.[28] The highly-ordered architectures of such intriguing materials possess many fascinating features like low framework density, tuneable porosity, high thermal and chemical stabilities as well as easy functionalization.[29] These remarkable characteristics make them serve as a uniquely ideal platform for diverse applications.[30] Many studies have shown that COFs can be regarded as promising materials for gas storage (such as H_2, CH_4 and CO_2)[31–34] and separation (such as CO_2/CH_4 and CO_2/N_2).[35–38] To the best of our knowledge, studies on COFs for iodine capture are still very scarce,[17] although some amorphous porous organic materials have been examined for this purpose.[16,39] Thus, it is quite necessary to put more efforts into this aspect of COF research.

In light of the context described above, a large-scale computational study was conducted in this work to explore the structure–property relationships of COFs for the adsorption of both I_2 and CH_3I, using a database of 187 materials collected from the literature. For a practical application, screening COFs under the real conditions of a given system is essential. Thus, the adsorption behaviours of the two iodic species in all the COFs were investigated at 423 K and ambient pressure. Two COFs were identified to respectively have the highest adsorption capacities for I_2 and CH_3I compared to other solid adsorbents reported to date. The information obtained in this work may provide useful guidance for the design and synthesis of new materials for iodine capture applications.

Models and computational methods

COF structures

To build a representative database, 187 COFs that cover most of synthesized materials were collected and their guest-free crystalline structures were constructed according to the respective experimental studies. For those COFs reported without detailed atomic coordinate information, their structures were constructed following the structure information provided in the corresponding synthetic studies. The so-built database contains 19 3D-COFs with **ctn**, **bor**, **dia**, and **pts** topologies, and 168 2D-COFs with **hexagonal**, **square**, **triangular** and **hybrid** pores. Such a large database containing diversified structures can lay a foundation for exploring the structure–property relationships of COFs for iodine capture. The related structural descriptors of these COFs, including pore diameter, surface area, and free volume, were calculated using the open source package Zeo++.[40] A complete list of the studied COFs and their structural features are given in Table S1 in the ESI.†

Interatomic potentials

In this study, the adsorbate–adsorbate and adsorbate–COF interactions were described using a combination of Lennard-Jones (LJ) and Coulombic potentials. The I_2 molecule was modelled as a spherical model with the LJ potential parameters taken from the literature,[41] which were derived from the viscosity calculation of pure I_2. The CH_3I molecule was represented using an explicit rigid model with five charged LJ interaction sites located on each atom, for which the potential parameters were taken from the work of Crone-Munzebrock and Doge.[42] For the COFs studied, an atomistic representation was used for all of them. The LJ potential parameters were taken from the universal force field (UFF),[43] and the partial charges of these atoms were calculated by the charge equilibration (QEq) method, using the code developed by Wells *et al.*[44] All the potential parameters for the adsorbates and COFs are provided in the ESI.† All the LJ cross interaction parameters were determined by the Lorentz–Berthelot mixing rule. As far as we know, no experimental data are available at the moment for the adsorption of gaseous I_2 and CH_3I in COFs with crystalline structures, although there are some experimental studies on several porous organic materials that are essentially amorphous. Thus, it is computationally difficult to directly confirm the reliability of these force fields. However, the above set of force fields has been widely used to study I_2 adsorption in various MOFs[26,27] and good agreements have also been found between simulation and experimental results.[20,21] In addition, although the diatomic model has been used to study I_2 adsorption in MOFs,[21] we found that there are significant deviations between the simulation results and experimental data.[21,22] Therefore, it may be reasonably assumed that the above sets of force fields are applicable to study the performance of COFs for iodine capture.

Simulation details

Grand canonical Monte Carlo (GCMC) simulations were performed to investigate the adsorption of gaseous I_2 and CH_3I in the COFs at 423 K and 1 bar, using our in-house code HT-CADSS (High-throughput-based Complex Adsorption and

Diffusion Simulation Suite). During the simulations, molecules involve four types of trials: attempts (i) to displace a molecule (translation or rotation), (ii) to regrow a molecule at a random position, (iii) to create a new molecule, and (iv) to delete an existing molecule. All of the COFs were treated as rigid frameworks with atoms frozen at their crystallographic positions. A cutoff distance was set to 14.0 Å for the LJ interactions, while the long-range electrostatic interactions were handled using the Ewald summation technique. Periodic boundary conditions were considered in all three dimensions. Each run consisted of 1×10^7 steps to ensure equilibration, followed by 1×10^7 steps to sample the desired thermodynamic properties. Besides the adsorption amount, another important thermodynamic quantity of interest that can be obtained from a GCMC simulation is the isosteric heat of adsorption (Q_{st}). According to the ensemble theory, it could be calculated from[45]

$$Q_{st} = RT - \frac{\langle U_{ff} N\rangle - \langle U_{ff}\rangle\langle N\rangle}{\langle N^2\rangle - \langle N\rangle\langle N\rangle} - \frac{\langle U_{fm} N\rangle - \langle U_{fm}\rangle\langle N\rangle}{\langle N^2\rangle - \langle N\rangle\langle N\rangle}$$

where the brackets <…> denote the ensemble average, R is the gas constant, and N is the number of molecules adsorbed. The first and second terms are the contributions from the molecular thermal energy and adsorbate–adsorbate interaction energy U_{ff}, respectively, while the remaining term is the contribution from the adsorbate–adsorbent interaction energy U_{fm}. In this study, the contributions for the Q_{st} from the second and third terms are denoted as $Q_{st,ff}$ and $Q_{st,fm}$, respectively.

Results and discussion

Iodine adsorption

To obtain general knowledge of the structure–property relationships of COFs for iodine capture, the adsorption capacities of the 187 COFs examined in this work were firstly correlated with their structure features. To achieve high I_2 uptake, the results shown in Fig. 1a indicate that the optimum value for the largest cavity diameter (LCD) of COFs is around 24 Å. Fig. 1 also shows that a larger accessible surface area (S_{acc}) or void fraction (φ) of COFs will generally lead to a higher I_2 uptake.

Table S5 in the ESI† presents the 10 top-performing COFs identified from our database for I_2 adsorption. It can be found that 3D-COFs with structures having **ctn**, **bor**, **dia**, and **pts** topologies appear at the top of the list, suggesting the advantage of 3D-COFs in I_2 adsorption. In addition, 2D-COFs with **hexagonal** and **square** pores also show considerably high I_2 uptake. The preferred adsorption of I_2 in the COFs with mesoporous structures reminds us that the interactions between the guest molecules may dominate the adsorption behaviour of I_2 in these materials. To validate this speculation, we further calculated the isosteric heats of adsorption of I_2 in the top 10 COFs at 423 K and 1 bar, as shown in Fig. 2. The results show that the contributions ($Q_{st,ff}$) from the interactions between I_2 molecules are indeed much higher than those ($Q_{st,fm}$) between I_2 molecules and the COF frameworks. Actually, Hughes *et al.*[20] previously

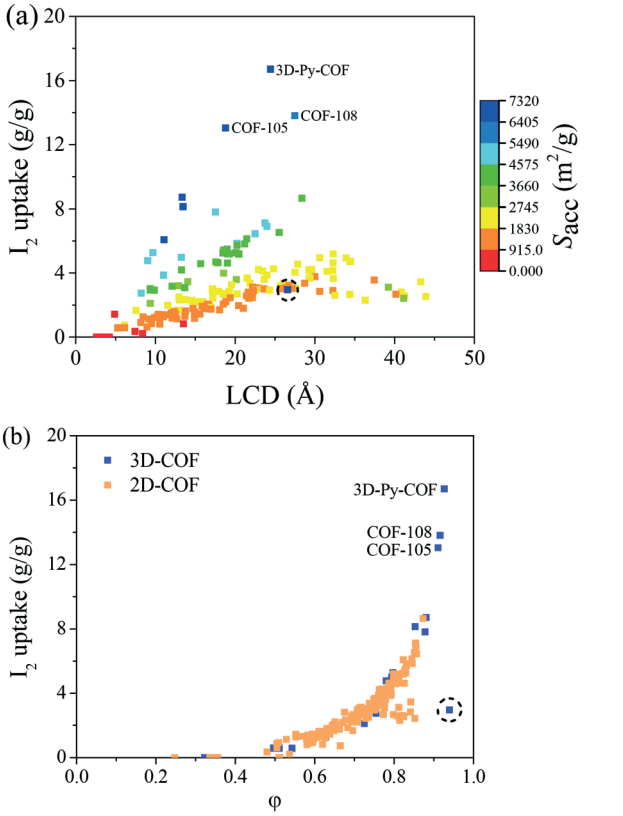

Fig. 1 Structure–property relationships of I_2 adsorption in COFs. (a) Relationship between the LCD (largest cavity diameter) of COFs and the I_2 uptake, colored by material surface area. (b) Relationship between the φ (void fraction) value of COFs and the I_2 uptake. The blue point enclosed by the dashed circles in the two figures corresponds to the material PI-COF-5 discussed in this work.

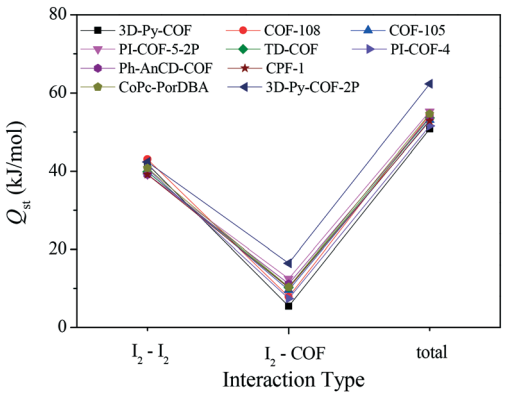

Fig. 2 Isosteric heats of adsorption of I_2 in the top 10 COFs identified from our database. In the abscissa, I_2–I_2 represents the contribution ($Q_{st,ff}$) from the interactions between I_2 molecules, I_2-COF represents the contribution ($Q_{st,fm}$) from the interactions between I_2 and COF frameworks, and total represents the total heat of adsorption. Simulation conditions: 423 K and 1 bar.

made the same speculation from their experimental study of I_2 adsorption in ZIF-8, but without giving direct evidence. To understand the adsorption behaviour of I_2 in the top-performing COFs at a molecular level, the microscopic adsorption mechanisms of this guest species were further examined. For this

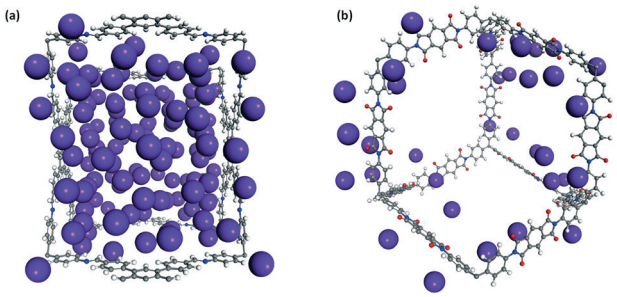

Fig. 3 I_2 adsorption configurations in the structures of: (a) 3D-Py-COF and (b) PI-COF-5. Frameworks are displayed in ball-and-stick style (H, white; C, grey; N, blue). The violet spheres displayed in space-fill style represent the I_2 molecules.

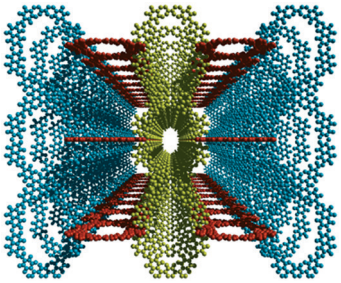

Fig. 4 Structure of the newly designed 3D-Py-COF-TANM.

purpose, a snapshot of I_2 adsorbed in 3D-Py-COF identified with the best performance is shown in Fig. 3a as an example. One can observe that I_2 molecules can fill the entire pore space of the material and are also inclined to form cluster-like structures due to the strong interactions between them.

However, the strong interactions between I_2 molecules themselves do not mean that the I_2 can be highly adsorbed in any COFs with high void fraction. For example, the blue point enclosed by the dashed circle in Fig. 1 corresponds to PI-COF-5. This 3D material has similar structural features (pore size, surface area and void fraction) to those of the best performing COF 3D-Py-COF, but its I_2 uptake is very low. A detailed comparison of the two COFs is shown in Table 1. It can be seen that the $Q_{st,ff}$ value in PI-COF-5 is much lower than that in 3D-Py-COF, resulting in a sharp contrast that PI-COF-5 can only have a small adsorption amount of I_2 and the molecules are mainly adsorbed near the framework, while the void space of 3D-Py-COF is almost fully occupied by I_2 molecules. By examining the structural features of the two materials, the biggest difference lies in their different topologies. The structure of 3D-Py-COF has a **pts** topology with square-like pores in which the significant confinement effects result in a very compact encapsulation of I_2 molecules. In comparison, the diamond-like structure of PI-COF-5 is connected by linear ligands, and thus its thin skeleton cannot lead to good packing behaviour of I_2 molecules in the pore space. To further confirm these observations, we manually replaced the building block of tetra(*p*-aminophenyl)-methane (TAPM) in 3D-Py-COF by tetra(*p*-amino naphthyl) methane (TANM) to construct a **pts** framework named 3D-Py-COF-TANM, for which the optimized structure is shown in Fig. 4. The simulation result shows that this new COF at 423 K and 1 bar has an uptake of about 19.9 g g^{-1}, exceeding the performance of all the 187 COFs in our database. The lattice parameters and the detailed atomic coordinates for the 3D-Py-COF-TANM structure are provided in Table S6 in the ESI.† As can be seen from Table 1, the $Q_{st,ff}$ and the $Q_{st,ff}/Q_{st,fm}$ of 3D-Py-COF-TANM are both higher than those of 3D-Py-COF, suggesting that the strong interactions between I_2 molecules play a more dominant role in the adsorption of I_2 in 3D-Py-COF-TANM. In addition, except that the two COFs have the same topology, 3D-Py-COF-TANM has larger pore size and surface area than 3D-Py-COF. Therefore, 3D-Py-COF-TANM retains the characteristics of better adsorption environments, leading to a higher I_2 uptake.

Our screening results show that the best existing COF for I_2 capture is 3D-Py-COF, and its adsorption capacity (16.7 g g^{-1}) is significantly higher than those reported for the benchmark zeolites under similar conditions, such as AgX – silver-exchanged faujasite (0.20 g g^{-1}) and mordenite (0.17 g g^{-1}).[5] Actually, Fig. 1 shows that many COFs can surpass the performance of these typical zeolites and other amorphous porous organic frameworks like PAF-24 (2.76 g g^{-1}).[16] In addition, by surveying related studies on MOFs for I_2 capture, the best MOF reported so far, to the best of our knowledge, is the material NU-110 identified computationally,[26] which exhibits an uptake of 13.1 g g^{-1} for I_2 adsorption at 298 K and 1 bar. To directly compare with this MOF, we also performed molecular simulations to examine the performance of the 187 COFs under the conditions of 298 K and 1 bar, as shown in Fig. S1 in the ESI.† Evidently, there are three COFs (3D-Py-COF, COF-108 and COF-105) that can outperform NU-110, and 3D-Py-COF still has the highest uptake (19.8 g g^{-1}) among the examined COFs. It can be expected that NU-110 will have a lower uptake at 423 K and 1 bar (actually 10.5 g g^{-1}). Considering the good performance of 3D-Py-COF with **pts** topology, we further performed GCMC simulations to examine the I_2 uptakes of MOFs with the same topology. For this purpose, 12 MOF structures that have large accessible surface areas (ranging from 2213 to 5353 m^2 g^{-1}) and high void fractions (ranging from 0.65 to 0.88) were extracted from the Cambridge Structural Database (CSD). As can be seen from the results given in Table S7 in the ESI,† the best MOF is FEBXIV

Table 1 Structural features and adsorption properties (423 K and 1 bar) of 3D-Py-COF, PI-COF-5 and 3D-Py-COF-TANM

Material	Topology	LCD (Å)	S_{acc} (m^2 g^{-1})	φ	Q_{st} (kJ mol^{-1})	$Q_{st,ff}$ (kJ mol^{-1})	$Q_{st,fm}$ (kJ mol^{-1})	$Q_{st,ff}/Q_{st,fm}$	I_2 uptake (g g^{-1})
3D-Py-COF	**pts**	24.4	7229	0.93	50.8	41.8	5.4	7.7	16.7
PI-COF-5	**dia**	26.6	6479	0.94	28.3	9.1	15.6	0.6	3.0
3D-Py-COF-TANM	**pts**	26.5	7644	0.94	51.9	45.5	2.8	16.2	19.9

(CSD refcode) with a surface area of ~5200 m^2 g^{-1} and a void fraction of 0.88. This material exhibits an I_2 adsorption capacity of 7.1 g g^{-1}, which is much lower than that of 3D-Py-COF while comparable to the COFs with similar void fractions, as shown in Fig. 1b. The above results demonstrate that COFs can be regarded as very promising adsorbents for practical I_2 removal.

Methyl iodide adsorption

CH_3I is the main organic iodine substance in the vessel off-gas (VOG) released from used nuclear fuel (UNF) reprocessing plant, which is commonly considered more difficult to capture than elemental iodine.[9] Fig. 5 shows the simulated structure–property relationships of the 187 COFs for CH_3I adsorption at 423 K and 1 bar. It can be found that the pore diameter, surface area and void fraction of the well-performing COFs are about 10 Å, 5000 m^2 g^{-1} and 0.8, respectively. Table S8 in the ESI† lists the information of the top 10 COFs screened for methyl iodide adsorption. Although 2D-COFs account for nearly 90% of the COFs experimentally reported so far, 3D-COFs show much better performance than 2D-COFs. Noticeably, five 3D-COFs with **ctn** topology exhibit the best performance among the 187 COFs (see Table S8†). These COFs have different organic building blocks but share similar structural features, indicating the important role of pore morphology in CH_3I adsorption. PI-COF-4-2P and COF-300 are 3D-COFs with **dia** topology that have a suitable pore size of about 9 Å for CH_3I adsorption, which can be ascribed to the appropriate catenations of their frameworks.

Although the molecular size of CH_3I is slightly larger than that of I_2,[46] compared with the results shown in Fig. 1, Fig. 5 shows that the optimum pore size (as well as surface area and void fraction) of the top-performing materials for CH_3I adsorption is smaller than that for I_2 adsorption; moreover, the CH_3I uptakes in COFs are overall much lower than the I_2 uptakes. To understand the differences more clearly, the heats of adsorption of CH_3I in the top 10 COFs identified were calculated at 423 K and 1 bar, as shown in Fig. 6. Compared with the results for I_2 adsorption in COFs (Fig. 2), the $Q_{st,ff}$ is much closer to the $Q_{st,fm}$ in the situation of CH_3I adsorption. This suggests that the contribution from the interactions between a CH_3I molecule and the COF framework is as important as that from the interactions between CH_3I molecules. Furthermore, the $Q_{st,ff}$ of CH_3I is much lower than the $Q_{st,ff}$ of I_2, implying that CH_3I molecules are not inclined to aggregate in large amounts as I_2 molecules behave in COFs. In other words, achieving a high CH_3I uptake needs a framework with a strong confinement effect to restrict the CH_3I molecules.

To more intuitively explain the above phenomena, Fig. 7 shows a comparison of the microscopic configurations of CH_3I molecules adsorbed in COF-103 and 3D-Py-COF, respectively, with the best and poor performance. Obviously, the suitable pore size (9.7 Å) of COF-103 to a large extent can maximize the intermolecular interactions of CH_3I as well as those between CH_3I and the framework. For the case of 3D-Py-COF, it has a mesoporous structure with a pore size of 24.4 Å. Such an unfavourable void environment leads to the significantly weak interactions between CH_3I molecules ($Q_{st,ff}$ = 1.2 kJ mol^{-1}), resulting in the observation that few molecules are sparsely adsorbed near the pore walls while the more interior pore space is not useful.

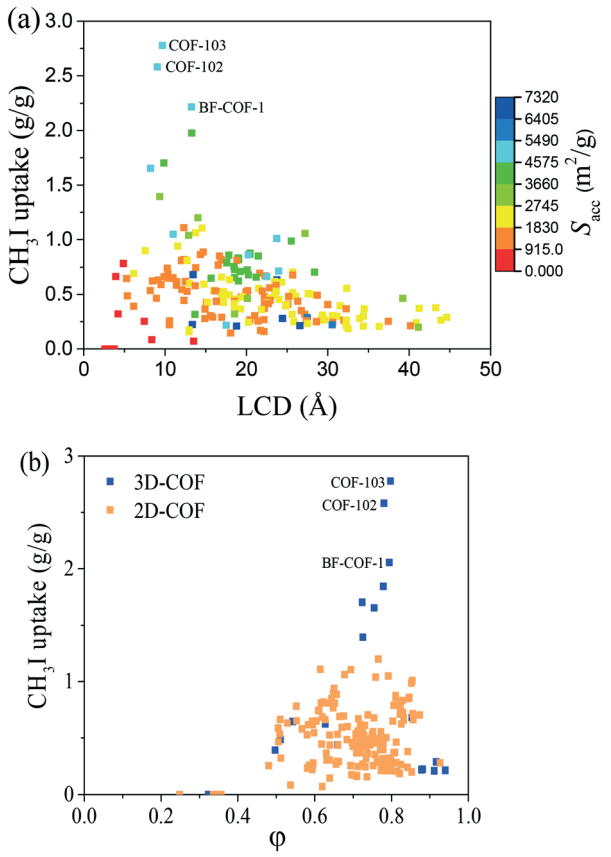

Fig. 5 Structure–property relationships of CH_3I adsorption in the 187 COFs. (a) Relationship between the LCD (largest cavity diameter) and CH_3I uptake, colored by material surface area. (b) Relationship between the φ (void fraction) and CH_3I uptake.

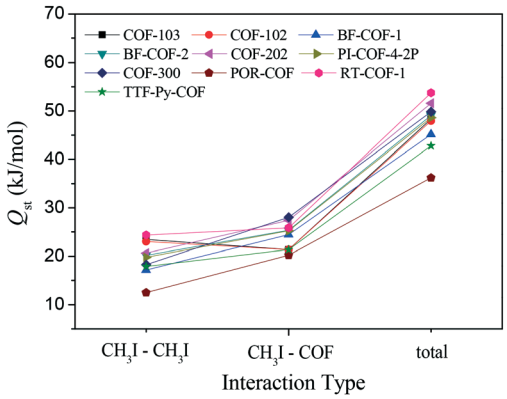

Fig. 6 Isosteric heats of adsorption of CH_3I in the top 10 COFs identified from the 187 materials. CH_3I–CH_3I represents the contribution ($Q_{st,ff}$) from the interactions between CH_3I molecules, CH_3I-COF represents the contribution ($Q_{st,fm}$) from the interactions between CH_3I and COF, and total represents the total heat of adsorption. Simulation conditions: 423 K and 1 bar.

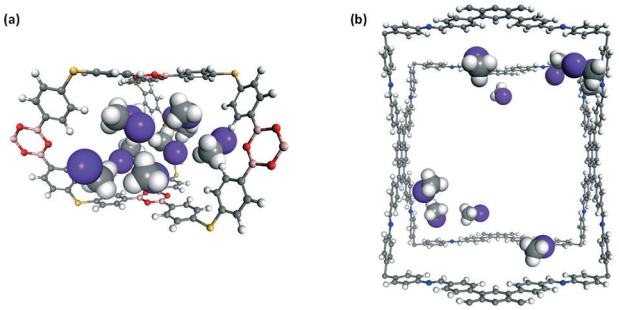

Fig. 7 CH_3I adsorption configurations in the structures of: (a) COF-103 and (b) 3D-Py-COF. Frameworks are displayed in ball-and-stick style (H, white; C, grey; N, blue; Si, yellow). The molecules displayed in space-fill style represent methyl iodide.

The importance of the confinement exerted by adsorbent frameworks also explains the superiority of 3D-COFs over 2D-COFs, since the 3D-grown framework not only can provide multiple surfaces for guest molecules to interact but can exert a stronger confinement effect on guest molecules from various directions. But, why do the COFs with **ctn** topology outperform the other 3D frameworks as reflected from Table S8 (see the ESI†) and Fig. 5? By comparing COF-202 (**ctn**, pore size of 9.9 Å) with PI-COF-4-2P (**dia**, pore size of 8.2 Å) which almost have the same CH_3I uptake (1.70 and 1.65 g g^{-1}, respectively), we can see that the **dia** topology needs a smaller pore to exert a comparative confinement on CH_3I adsorption compared with the **ctn** one. This from another side proves the stronger confinement ability of the **ctn**-type framework. As for other 3D-COFs, their unsatisfactory performance can be attributed to the overly large or overly small pore sizes, such as NPNs (**dia**, ~6 Å), COF-105 (**bor**, 19 Å) and PI-COF-5-2P (**pts**, 14 Å). At the moment, studies of CH_3I capture using adsorbents are mainly focused on activated carbons, alumina and zeolites. Compared with these traditional materials, the top three COFs (COF-103, COF-102 and BF-COF-1) show significantly better adsorption performance, as shown in Table S9 in the ESI.†

Conclusions

In this work, a large-scale computational screening study was for the first time performed to evaluate the performance of a diverse set of 187 experimental COFs for gaseous I_2 and CH_3I adsorption at 423 K and 1 bar, which are the more practical conditions related to the treatment of radioactive iodic contaminants produced from the nuclear industry. The results show that 3D-COFs have better performance than 2D-COFs for the capture of both I_2 and CH_3I. A monotonically increasing relationship was observed between the I_2 uptake and the void fraction of COFs but with the optimal pore size centred at around 24 Å. 3D-Py-COF was identified as the best adsorbent for I_2 capture with an I_2 uptake of 16.7 g g^{-1}, which is higher than any material's capacity reported so far. In addition, the intermolecular interactions of I_2 were found to provide the dominant driving force for I_2 adsorption. Based on the obtained structure–property relationship, a new 3D-COF with an even higher I_2 uptake of 19.9 g g^{-1} was designed. For CH_3I adsorption, there is no monotonous relationship existing between the adsorption capability and the structural features of COFs. A series of 3D-COFs with **ctn** topology having a pore size of about 9 Å were identified as the top-performing materials. Among them, COF-103 is the best material with a CH_3I uptake of 2.8 g g^{-1}, which is significantly higher than those of traditional adsorbents like activated carbons, alumina and zeolites. The results provided in this work can give guidance for experimental efforts in seeking advanced materials for I_2 and CH_3I adsorption, as well as can facilitate the practical applications of COFs.

Acknowledgements

This work was supported by the Natural Science Foundation of China (No: 21536001) and the National Key Research Program of China (2016YFA0201701).

References

1 S. Chu, *Nature*, 2012, **488**, 294.
2 A. Almansoori and A. Betancourt-Torcat, *Appl. Energy*, 2015, **148**, 234.
3 S. U. Nandanwar, K. Coldsnow, V. Utgikar, P. Sabharwal and D. E. Aston, *Chem. Eng. J.*, 2016, **306**, 369.
4 T. M. Nenoff, M. A. Rodriguez, N. R. Soelberg and K. W. Chapman, *Microporous Mesoporous Mater.*, 2014, **200**, 297.
5 D. R. Haefner and T. J. Tranter, *Methods of Gas Phase, Capture of Iodine from Fuel Reprocessing Off-Gas: A Literature Survey; INL/EXT-07-12299*, Idaho National Laboratory, Idaho Falls, ID, 2007.
6 G. Massasso, J. Long, J. Haines, S. Devautour-Vinot, G. Maurin, A. Grandjean, B. Onida, B. Donnadieu, J. Larionova, C. Guérin and Y. Guari, *Inorg. Chem.*, 2014, **53**, 4269.
7 C. M. González-García, J. F. González and S. Román, *Fuel Process. Technol.*, 2011, **92**, 247.
8 K. W. Chapman, P. J. Chupas and T. M. Nenoff, *J. Am. Chem. Soc.*, 2010, **132**, 8897.
9 S. H. Bruffey, R. T. Jubin and J. A. Jordan, *Organic Iodine Adsorption by AgZ under Prototypical Vessel off-Gas Conditions: Fuel Cycle Research & Development*, U.S. DOE, FCRD-MRWFD-2016-000357, ORNL/TM-2016/568, 2016.
10 J. Zhou, S. Hao, L. Gao and Y. Zhang, *Ann. Nucl. Energy*, 2014, **72**, 237.
11 H. Sun, P. La, Z. Zhu, W. Liang, B. Yang and A. Li, *J. Mater. Sci.*, 2015, **50**, 7326.
12 C. Herdes, C. Prosenjak, S. Román and E. A. Müller, *Langmuir*, 2013, **29**, 6849.
13 B. J. Riley, J. Chun, J. V. Ryan, J. Matyas, X. S. Li, D. W. Matson, S. K. Sundaram, D. M. Strachan and J. D. Vienna, *RSC Adv.*, 2011, **1**, 1704.
14 Y. Lu, H. Liu, R. Gao, S. Xiao, M. Zhang, Y. Yin, S. Wang, J. Li and D. Yang, *ACS Appl. Mater. Interfaces*, 2016, **8**, 29179.

15 B. Riebe, S. Dultz and C. Bunnenberg, *Appl. Clay Sci.*, 2005, **28**, 9.
16 Z. Yan, Y. Yuan, Y. Tian, D. Zhang and G. Zhu, *Angew. Chem., Int. Ed.*, 2015, **54**, 12733.
17 B. T. Hertzsch, C. Gervais, J. Hulliger, B. Jaeckel, S. Guentay, H. Bruchertseifer and A. Neels, *Adv. Funct. Mater.*, 2006, **16**, 268.
18 J. Duan, C. Zou, Q. Li and W. Jin, *CrystEngComm*, 2015, **17**, 8226.
19 G. Massasso, J. Long, J. Haines, S. Devautour-Vinot, G. Maurin, A. Grandjean, B. Onida, B. Donnadieu, J. Larionova, C. Guérin and Y. Guari, *Inorg. Chem.*, 2014, **53**, 4269.
20 J. T. Hughes, D. F. Sava, T. M. Nenoff and A. Navrotsky, *J. Am. Chem. Soc.*, 2013, **135**, 16256.
21 D. F. Sava, M. A. Rodriguez, K. W. Chapman, P. J. Chupas, J. A. Greathouse, P. S. Crozier and T. M. Nenoff, *J. Am. Chem. Soc.*, 2011, **133**, 12398.
22 D. F. Sava, K. W. Chapman, M. A. Rodriguez, J. A. Greathouse, P. S. Crozier, H. Zhao, P. J. Chupas and T. M. Nenoff, *Chem. Mater.*, 2013, **25**, 2591.
23 C. Falaise, C. Volkringer, J. Facqueur, T. Bousquet, L. Gasnotb and T. Loiseaua, *Chem. Commun.*, 2013, **49**, 10320.
24 V. Safarifard and A. Morsali, *CrystEngComm*, 2014, **16**, 8660.
25 A. S. Munn, F. Millange, M. Frigoli, N. Guillou, C. Falaise, V. Stevenson, C. Volkringer, T. Loiseau, G. Cibin and R. I. Walton, *CrystEngComm*, 2016, **18**, 8108.
26 B. Assfour, T. Assaad and A. Odeh, *Chem. Phys. Lett.*, 2014, **610**, 45.
27 Y. Yuan, X. Dong, Y. Chen and M. Zhang, *Phys. Chem. Chem. Phys.*, 2016, **18**, 23246.
28 A. P. Côté, A. I. Benin, N. W. Ockwig, M. O'Keeffe, A. J. Matzger and O. M. Yaghi, *Science*, 2005, **310**, 1166.
29 B. P. Biswal, S. Chandra, S. Kandambeth, B. Lukose, T. Heine and R. Banerjee, *J. Am. Chem. Soc.*, 2013, **135**, 5382.
30 X. Feng, X. Ding and D. Jiang, *Chem. Soc. Rev.*, 2012, **41**, 6010.
31 E. Tylianakis, E. Klontzasa and G. E. Froudakis, *Nanoscale*, 2011, **3**, 856.
32 J. L. Mendoza-Cortes and W. A. Goddard III, *J. Phys. Chem. Lett.*, 2012, **3**, 2671.
33 R. L. Martin, C. M. Simon, B. Medasani, D. K. Britt, B. Smit and M. Haranczyk, *J. Phys. Chem. C*, 2014, **118**, 23790.
34 R. Babarao and J. Jiang, *Energy Environ. Sci.*, 2008, **1**, 139.
35 M. Tong, Q. Yang, Y. Xiao and C. Zhong, *Phys. Chem. Chem. Phys.*, 2014, **16**, 15189.
36 M. Tong, Q. Yang and C. Zhong, *Microporous Mesoporous Mater.*, 2015, **210**, 142.
37 Z. Xiang, R. Mercado, J. M. Huck, H. Wang, Z. Guo, W. Wang, D. Cao, M. Haranczyk and B. Smit, *J. Am. Chem. Soc.*, 2015, **137**, 13301.
38 R. Babarao, R. Custelcean, B. P. Hay and D.-E. Jiang, *Cryst. Growth Des.*, 2012, **12**, 5349.
39 S. A. Y. Zhang, Z. Li, H. Xia, M. Xue, X. Liu and Y. Mu, *Chem. Commun.*, 2014, **50**, 8495.
40 T. F. Willems, C. H. Rycroft, M. Kazi, J. C. Meza and M. Haranczyk, *Microporous Mesoporous Mater.*, 2012, **149**, 134.
41 J. O. Hirschfelder, C. F. Curtiss, R. B. Bird and M. G. Mayer, *Molecular theory of gases and liquids*, Wiley, New York, 1954.
42 H. Crone-Munzebrock and G. Doge, *Ber. Bunsenges. Phys. Chem.*, 1990, **94**, 297.
43 A. K. Rappe, C. J. Casewit, K. S. Colwell, W. A. Goddard III and W. M. Skiff, *J. Am. Chem. Soc.*, 1992, **114**, 10024.
44 B. A. Wells, C. D. Bruin-Dickason and A. L. Chaffee, *J. Phys. Chem. C*, 2015, **119**, 456.
45 Q. Yang, D. Liu, C. Zhong and J. Li, *Chem. Rev.*, 2013, **113**, 8261.
46 R. D. Scheele, L. L. Burger and C. L. Matsuzaki, *Methyl iodide sorption by reduced silver mordenite*, Report No. OPNL-4489, Pacific Northwest Laboratory, Richland, WA, 1983.

